limited by the two red dashed lines in Fig. 5.4 (c) in which the shear strain is localized. As a result, the contrast between the effective strain levels within and outside the macro-band is huge.

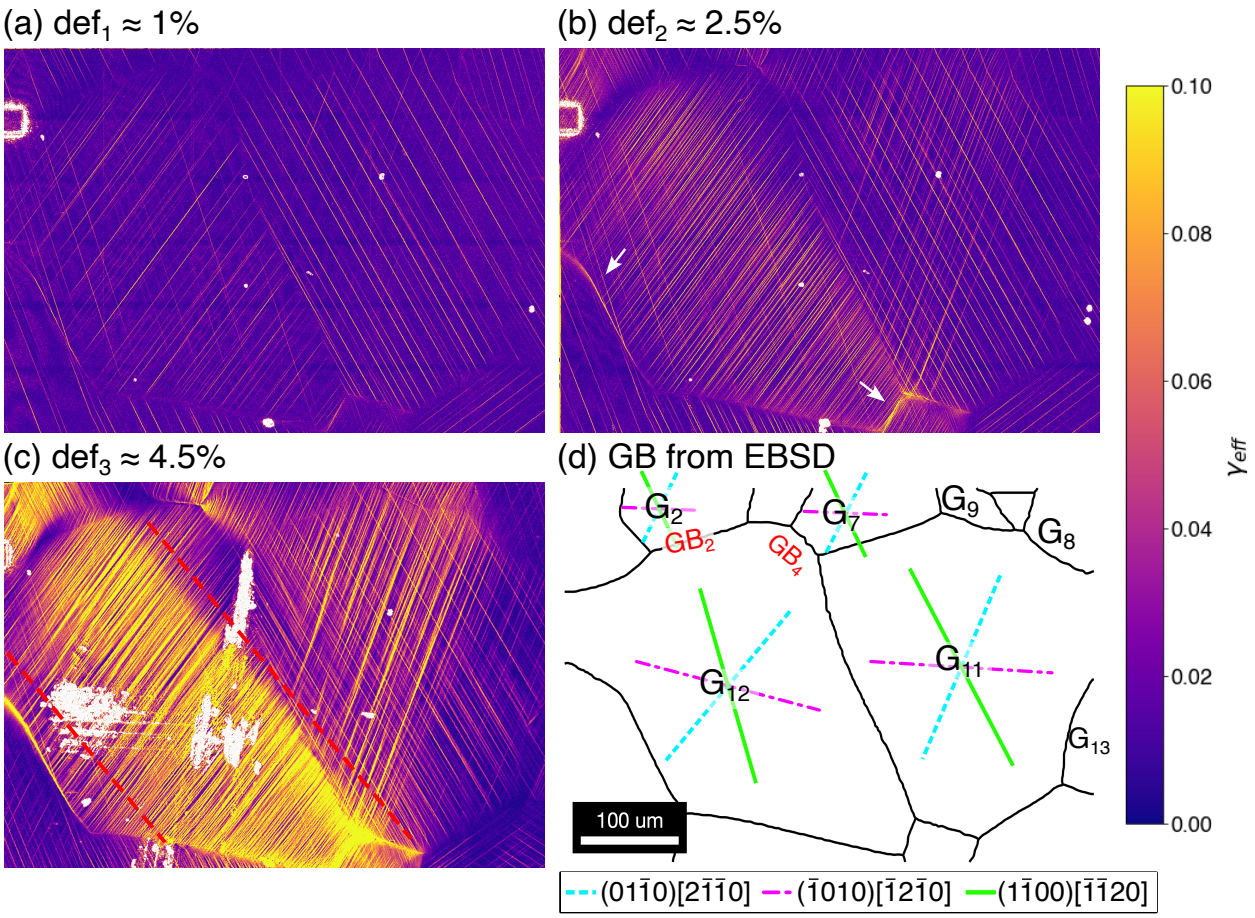

Figure 5.4: Effective shear strain maps acquired by HRDIC in the sample within sub-region 1. The correlated maps correspond to three deformation steps at (a) 1%, (b) 2.5%, and 4.5% plastic deformation. The white pixels in the maps correspond to non-correlated points caused by surface scratches and dirt deposited onto the gold nano-speckle pattern. The white arrows in (b) highlight strain concentrations close to GB and triple junctions. The red dashed lines in (c) delimit a macro-strain band. (d) GB map obtained from EBSD before deformation. The main grains and GB of study have been labeled, and the theoretical prismatic slip traces have been drawn at the center of the grains.

The effective shear strain distribution acquired in sub-region 2 is displayed in Fig. 5.5 for the three plastic strains of 1% (a), 2.5% (b) and 4.5% (c), whereas (d) presents a GB map with labeled grains and GBs of study in which the theoretical prismatic slip traces have been drawn at the center of the grains.

As observed in Fig. 5.5 (d), all slip bands are identified as prismatic, and the slip activity and intensity increase with plastic deformation. Several strain concentrations appear at 2.5% plastic deformation, especially at the triple junctions, and they are highlighted

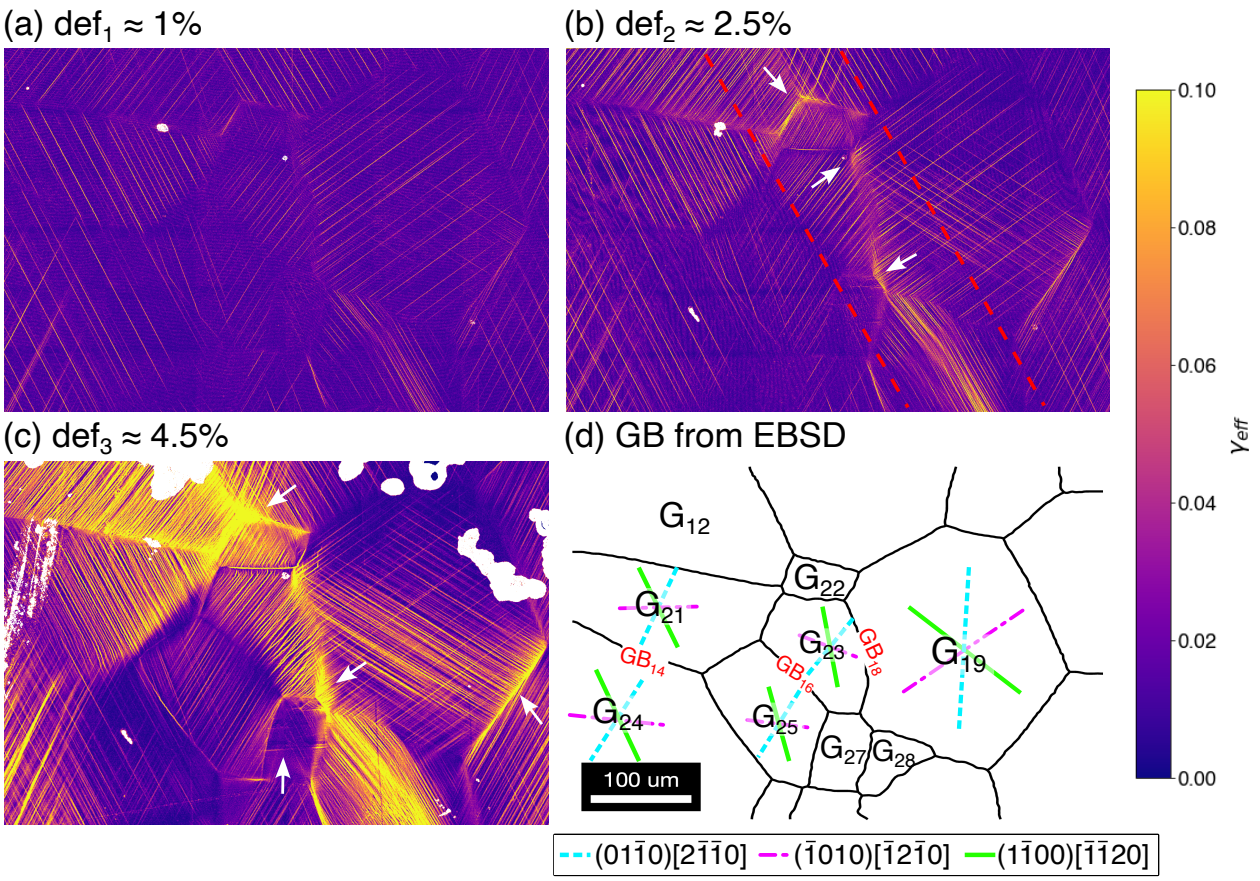

Figure 5.5: Effective shear strain maps, γ_{eff}, obtained by HRDIC in the ROI within subregion 2. The correlated maps correspond to three deformation steps at (a) 1%, (b) 2.5%, and 4.5% applied plastic deformation. The white pixels in the maps correspond to non-correlated points caused by surface scratches and dirt deposited onto the gold nano-speckle pattern. The white arrows in (b) and (c) highlight different strain concentrations close to GBs and triple junctions. The red dashed lines in (b) delimit a macro-strain band. (d) GB map obtained from the EBSD map before deformation. The main grains and GB of study have been labeled, and the theoretical prismatic slip traces have been drawn at the center of the grains.

with white arrows in Fig. 5.5 (b). The shear strain distribution shows the localization of the plastic deformation along a strain band that goes through grains G_{22}, G_{23}, and G_{28}, delimited by the two red dashed lines in Fig. 5.5 (b). The strain localization within the band increases with the applied strain, as shown in Fig. 5.5 (c), while the strain did not increase that much in the neighborhood of the macro band and in the surrounding grains (i.e. G_{25}). Furthermore, G_{22} undergoes an out-of-plane displacement to accommodate plastic deformation, as evidenced in the HRDIC maps after 2.5% and 4.5% deformation due to its small size and position within the macro-strain band. In contrast, G_{27} barely experienced plastic deformation at 2.5%, but deformation twinning was observed after 4.5% plastic deformation. This seems to indicate that G_{27} could not accommodate all plastic deformation within the macro-strain band region by slip, and thus twinning was activated

between 2.5% and 4.5% plastic deformation, leading to a relaxation in the shear strain, as observed in the third deformation map (Fig. 5.5 (c)).

The HRDIC maps acquired within the third sub-region of the ROI are presented in Fig. 5.6. Once again, all observed slip traces belong to prismatic planes, which increase in intensity and activity with applied deformation. Some shear strain concentrations at GBs are observed from the second deformation.

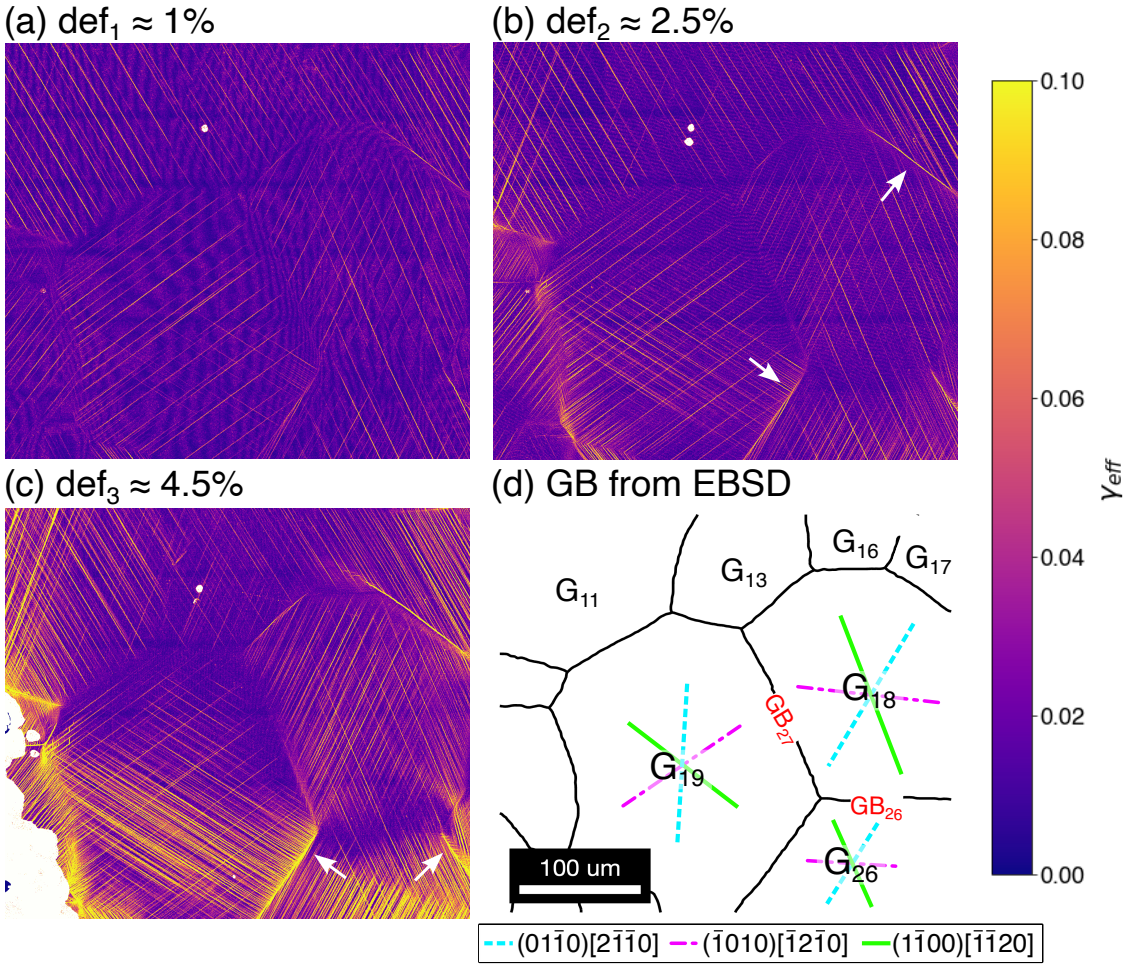

Figure 5.6: Effective shear strain maps acquired by HRDIC in the sample within sub-region 3. The correlated maps correspond to three deformation steps at (a) 1%, (b) 2.5%, and 4.5% plastic deformation. The white pixels in the maps correspond to non-correlated points caused by surface scratches and dirt deposited onto the gold nano-speckle pattern. The white arrows in (b) highlight strain concentrations close to GB and triple junctions. The red dashed lines in (c) delimit a macro-strain band. (d) GB map obtained from the EBSD map before deformation. The main grains and GB of study have been labeled, and the theoretical prismatic slip traces have been drawn at the center of the grains.

The occurrence of slip transfer/blocking across 28 GBs within the ROI was analyzed from the three effective shear strain maps for the three applied strain levels. The clear observation of the slip bands from the effective shear strain maps allowed us to reveal whether slip

transfer occurred at the GB, as revealed by the continuity between the slip traces across a GB. On the contrary, the discontinuity between the slip bands or the absence of slip traces at the GB region indicates slip blocking, and this conclusion can be supported by the presence of a strain concentration at the GB. Partial slip transfer can also be observed when just some slip bands are continuous across the GB or when the intensity of the slip bands significantly decreases a few microns away from the GB.

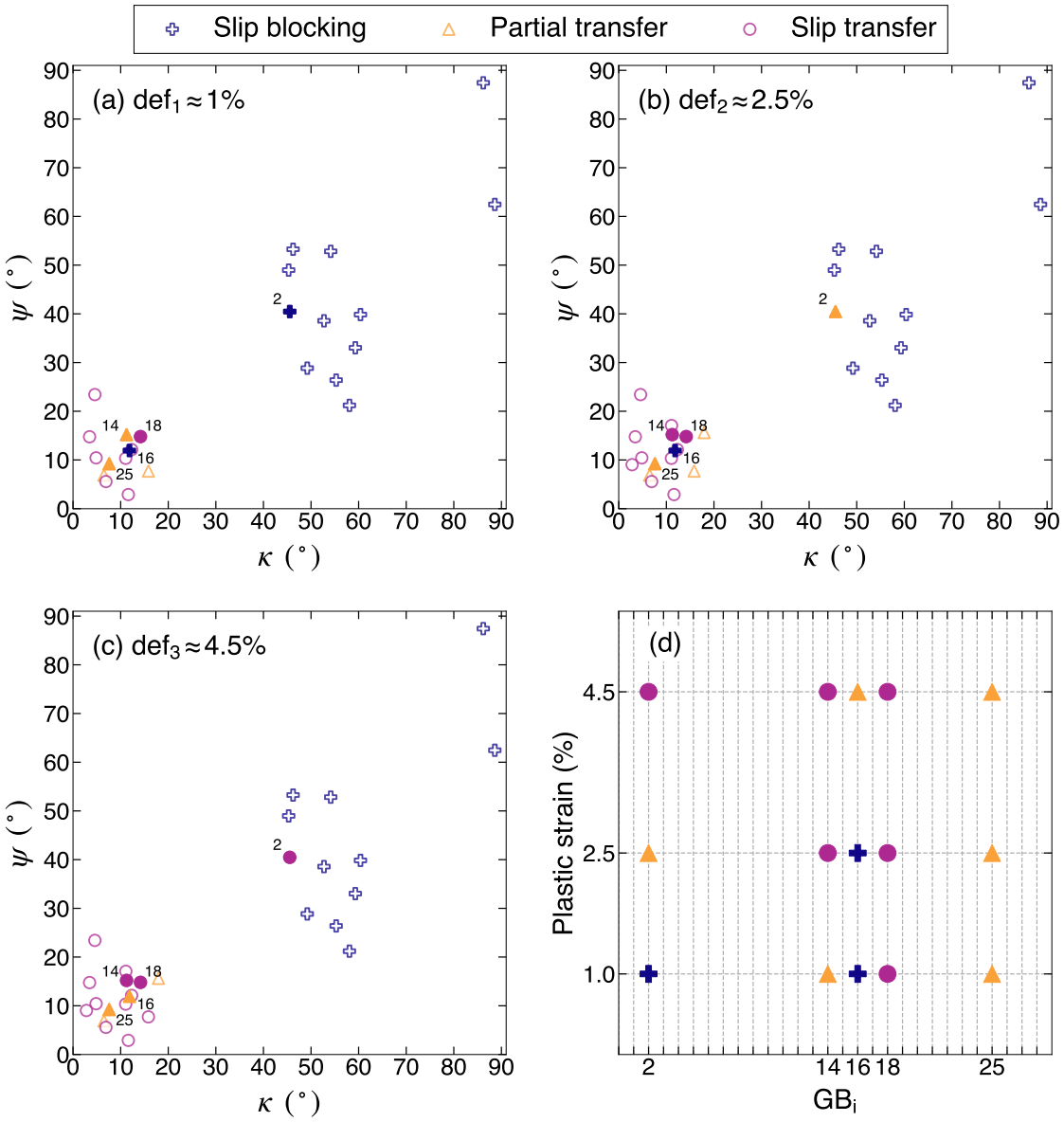

Figure 5.7: Influence of κ and ψ on slip transfer/blocking across the GBs as a function of the applied plastic deformation. (a) $\mathrm{def}_1 \approx 1\%$, (b) $\mathrm{def}_2 \approx 2.5\%$, and (c) $\mathrm{def}_3 \approx 4.5\%$. The GBs labeled with solid symbols will be analyzed in more detail in the next sections due to their unexpected slip transfer behavior. (d) Summary of the changes in the occurrence of slip transfer with plastic deformation in the selected GBs.

Once the active prismatic slip systems are identified, all the geometrical parameters that

characterize the alignment between the incoming and outgoing slip systems can be determined. The angles κ and ψ are obtained from the identification of the active prismatic slip planes, with κ as the angle between Burgers vectors and ψ as the angle between slip planes. However, the twist angle θ cannot be determined from surface observation only but needs the GB normal, which can only be obtained by 3D information about the orientation of the GB within the sample provided by DCT. The influence of κ and ψ on the occurrence of slip transfer across the GBs within the ROI as a function of plastic deformation is plotted in Fig. 5.7. The slip transfer events are indicated with dark pink circles, partial slip transfer with orange triangles, and slip blocking with blue crosses. Solid symbols indicate GBs that will be analyzed in more detail in Section 5.3.3.

The effect of the twist angle θ against the angle κ between Burgers vectors on slip transfer is plotted in Fig. 5.8 as a function of the applied plastic deformation. Most slip transfer and partial slip transfer events are located at low θ and κ, whereas slip blocking is associated with higher values. As already reported [131], the twist angle does not seem to play an important role in the occurrence of slip transfer, compared to the effect of the angle κ. .

As observed in Figs. 5.7 (a)-(c), most of the studied GBs fulfill the slip transfer criteria extensively reported in the literature for all applied deformations: slip transfer is favored when the slip systems across the GB are well aligned (low κ and low ψ). The partial slip transfer events are also located within the slip transfer region, which seems reasonable since these GBs can transfer slip to some extent.

Nevertheless, several GBs present an unforeseen slip transfer behavior depending on the applied plastic deformation. Five GBs have been selected for a deeper analysis due to this abnormal behavior. They are labeled in Figs. 5.7(a)-(c) and depicted with solid symbols. The summary of the slip transfer state (blocking, partial, or transfer) for these selected GBs is presented in Fig. 5.7(d) for the three applied deformations. GB_2, GB_{14}, and GB_{16} represent GBs whose slip transfer state evolves with plastic deformation. For instance, GB_2 evolves from slip blocking to partial slip transfer to full slip transfer with the applied plastic strain, even though there is a significant misalignment between the active slip systems. On the contrary, partial slip transmission is found in GB_{25} for all applied strain, even though the geometrical alignment makes it suitable for perfect slip transfer. Finally, although GB_{18} presents clear slip transfer from the lowest strain level, it has been selected for further analysis due to some unexpected plastic deformation mechanisms in its neighborhood due to its location within the macro-strain band influence region. These results suggest that the geometrical alignment between slip systems is not the only factor that plays a role in the occurrence or absence of slip transfer across GBs.

5.3.2 When slip transfer geometrical criteria work

Slip transfer was analyzed in more detail in some GBs where the classical geometrical criteria are fulfilled: slip transfers when the incoming and outgoing slip systems are well aligned, and slip is blocked when they are not. Several detailed sections of the effective shear strain maps within the ROI are depicted in Fig. 5.9, showing a close-up view of two different GBs (by rows) for the three applied deformations (by columns). The theoretical

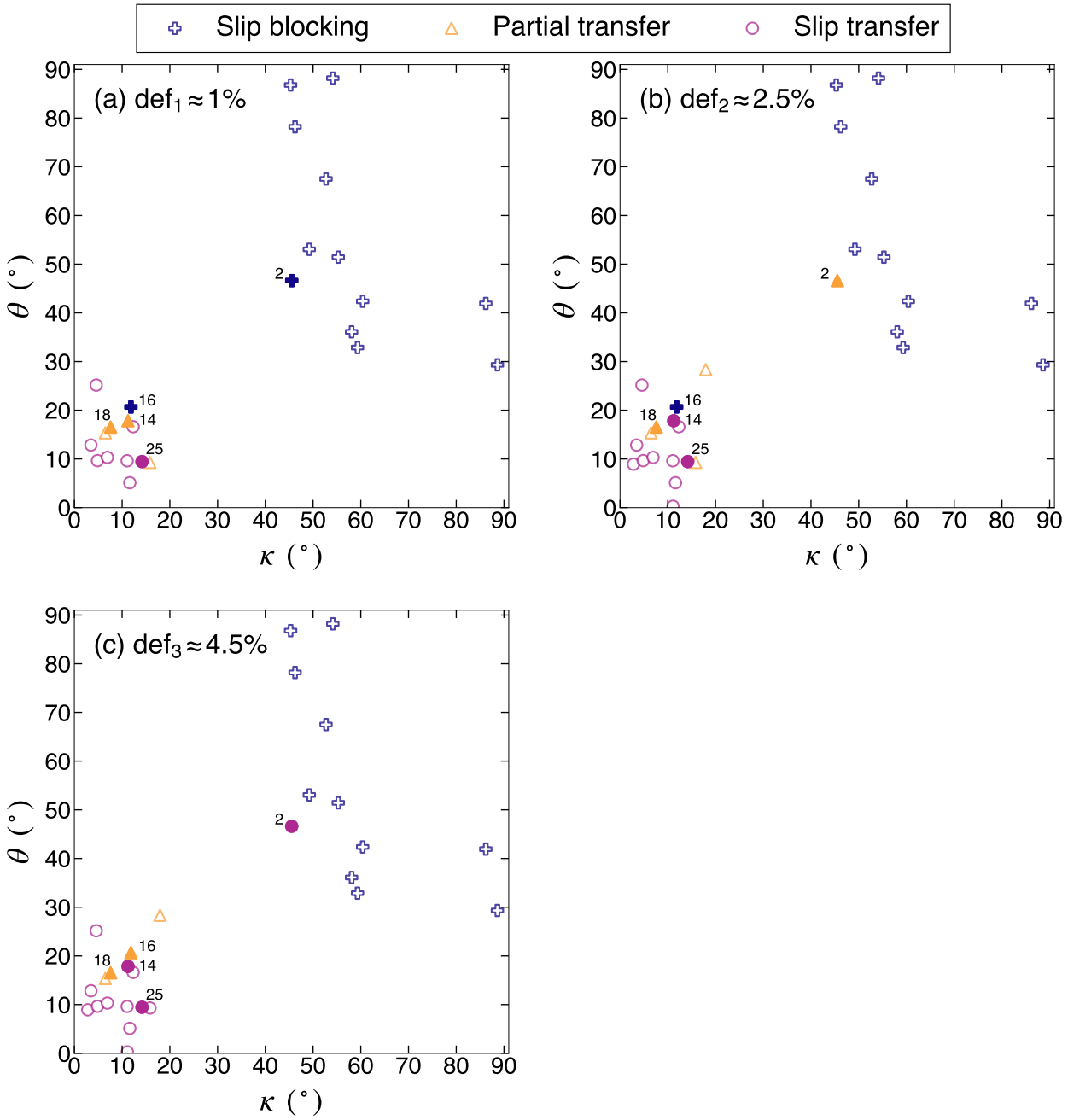

Figure 5.8: Influence of κ and θ on the occurrence of slip transfer/blocking across the analyzed GBs as a function of the applied plastic deformation. (a) $\mathrm{def}_1 \approx 1\%$, (b) $\mathrm{def}_2 \approx 2.5\%$, and (c) $\mathrm{def}_3 \approx 4.5\%$.

slip traces of the active prismatic planes have been drawn on top of the maps for slip system identification. The geometrical parameters and the values of selected slip transfer criteria (m', Δb, and LRB) have been calculated for the observed pairs of active slip systems across each GB (Table 5.1).

The first row of micrographs in Fig. 5.9 shows a case of convincing slip transfer across GB_4

from the lowest applied deformation (Fig. 5.9 (a)), where a pair of traces presents continuity across the boundary. The active slip systems in both grains across the boundary are uniquely identified as the $(01\bar{1}0)[2\bar{1}\bar{1}0]$ prismatic slip system, which is ranked first among the three possible prismatic slip systems according to their SF, as shown in Table 5.1. Due to its small misorientation angle, the slip systems across GB_4 are very well aligned, and κ and ψ are small, leading to high m' and low $\Delta b/b$. Furthermore, the twist angle θ calculated from the active slip planes and the GB normal is also low ($< 20°$), and so the LRB factor is also high. As observed in other studies [7, 24, 82, 130, 154], these results are all indicators of slip transfer across this GB. After the second applied deformation (Fig. 5.9 (b)), the number of slip bands and their intensity increase in both grains, especially in grain G_7, and hence more slip bands can go through the GB. In the third step of plastic deformation, the effective shear strain in the slip bands increases, and slip transfer is fairly evident all over the GB length. Moreover, there is no strain concentration at the GB (Fig. 5.9 (c)).

A clear slip blocking event is observed across GB_{27} in Fig. 5.9 (d)-(f), that presents a high misorientation angle Θ, as reported in Table 5.1. Double prismatic slip is observed in G_{18} and G_{19} after the first deformation step, and the active slip systems in each grain are the first and second according to their SF and all > 0.38. The slip bands that meet at the GB are the pink prismatic slip system $(\bar{1}010)[\bar{1}2\bar{1}0]$ in G_{19} (ranked second) and the blue prismatic slip system $(01\bar{1}0)[2\bar{1}\bar{1}0]$ (ranked first) in G_{18}. However, these slip systems are not adequately oriented for slip transmission, as shown in the angular parameters in Table 5.1, and slip transfer does not occur for any applied deformation. Furthermore, despite presenting slip blocking, there is only a slight strain concentration at the bottom region of this GB, which decreases as the distance to the triple point increases.

Table 5.1: Geometrical parameters and slip transfer criteria between the active prismatic slip systems for GB_4, and GB_{27}. The rank of the SF of the active prismatic slip system among the three possible planes is indicated between parenthesis and the SF is colored according to the active slip systems indicated in the legend in Fig. 5.9.

GB_i	$\mathrm{G_A}$	$\mathrm{G_B}$	$\mathrm{SF_A(R)}$	$\mathrm{SF_B(R)}$	Θ	κ	ψ	θ	m'	$\Delta b/b$	LRB
GB_4	7	12	0.45(1)	0.5(1)	13°	12.3°	12.1°	16.6°	0.96	0.21	0.94
GB_{27}	18	19	0.47(1)	0.43(2)	74.2°	54.1°	52.8°	88.2°	0.35	0.91	0.02

In summary, the likelihood of slip transfer across a GB increases when the active slip systems are geometrically well-aligned; otherwise, slip is blocked at the GB. Thus, the well-known geometrical criteria, m', Δb, and LRB, are generally good predictors for slip transfer across GBs.

5.3.3 When slip transfer geometrical criteria fail: the influence of local stress

As indicated in Fig. 5.7, several GBs within the ROI present an unexpected slip transfer behavior according to the conventional geometrical slip transfer criteria. As observed